Structural Wing-Fuselage Static Interaction by a Combined Method of Tests and Numerical Analyses

I. Kalev,* M. Baruch,† and E. Blass‡
Technion – Israel Institute of Technology, Haifa, Israel

The structural wing-fuselage interaction has a major influence on the Kfir aricraft stress distributions. A method that combines both numerical computations and separate full-scale nondestructive static tests of the wing and of the fuselage is described. The reasons for preferring such an approach over other possibilities are discussed. The method is composed of five main interdependent items as follows: 1) performance of static tests on a full-scale wing; 2) performance of static tests on a full-scale fuselage; 3) construction of finite-element model of the wing; 4) construction of finite-element models of the fuselage frames to which the wing is attached; and 5) computation of the wing-fuselage interaction using the force method and considering the wing and the fuselage as two substructures.

Nomenclature

b = equilibrium transformation matrix of the wing-fuselage attachment points, see Eq. (3)
$\bar{b}$ = statically determined wing reactions due to unit loads, see Eq. (12)
B.C. = boundary conditions
D = see Eq. (10)
d = see Eq. (11)
F = $\{F_1,\ldots, F_{12}\}$ = wing-fuselage interaction force vector, see Eq. (3)
F.E. = finite element
H = strain matrix due to unit loads, see Eq. (1)
P_0 = load vector, see Eq. (3)
R = wing reaction vector, see Eq. (1)
r = displacement vector at wing-fuselage attachment points, see Eq. (4)
U = displacement vector, see Eq. (5)
V = wing displacement vector due to fuselage flexibilities, see Eq. (13)
X = redundant force vector, see Eq. (2)
ϵ, ϵ_0 = strain vector, see Eq. (1)

Subscripts

f = due to redundant fuselage forces
f_0 = due to external loads acting on the fuselage
W = due to redundant wing forces
W_0 = due to external loads acting on the wing
δ = flexibility matrix, see Eqs. (5) and (7)

Superscript

T = transpose

Introduction

THE wings of the Kfir aircraft are connected to the fuselage at four discrete points. The attachment points are constructed so that the wing-fuselage structural interaction system is composed of twelve generalized forces and moments denoted in Fig. 1 as F_1 to F_{12}. Both the fuselage and the wings are flexible structures. To determine the real stress distributions in both the wing and the fuselage structures, the elastic coupling between the fuselage and wings should be considered.

This paper presents a method that combines both full-scale nondestructive static tests of the wing and of the fuselage and numerical computations. The experimental load conditions represent subsonic and supersonic symmetric maneuvers with a typical weight configuration. However, the final result of the method is to obtain the wing-fuselage structural interaction for any symmetric load condition. Antisymmetric

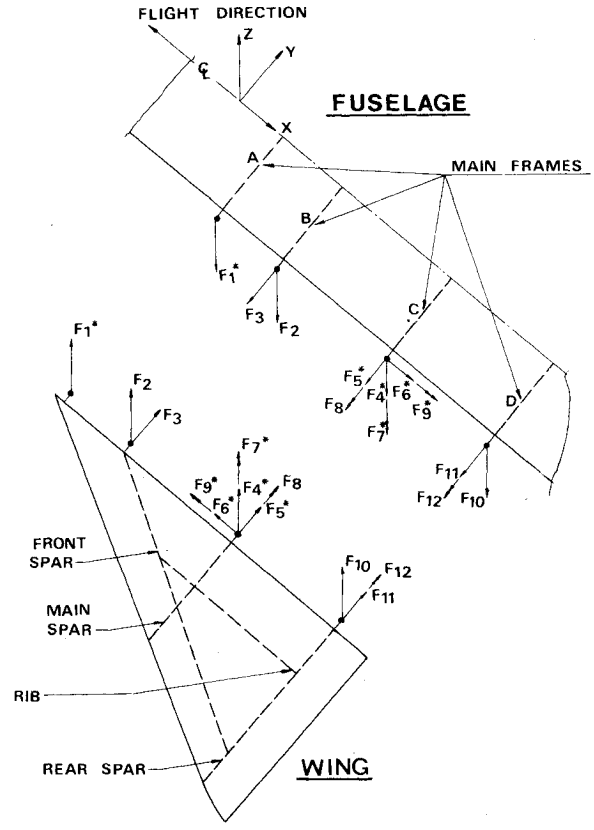

$F_1, F_2, \ldots F_{12}$ – WING–FUSELAGE INTERACTION FORCES

(*) – DENOTES THE CHOSEN STATICALLY–DETERMINATE FORCES

Fig. 1 Wing-fuselage interaction forces.

Received Aug. 26, 1976; revision received May 31, 1977.
Index categories: Structural Statics; Testing, Flight and Ground.
*Department of Structures, Faculty of Civil Engineering.
†Professor, Department of Aeronautical Engineering; now Visiting Professor at the Mechanics Department, University of Wisconsin-Milwaukee. Member AIAA
‡Department of Aeronautical Engineering.

load conditions have not been considered, but it would be possible to incorporate them by using a similar procedure of testing and numerical analyses. The experimental measurements include displacements, strains, and reactions. The reactions were obtained using strain gage installations calibrated on the wing structure. The numerical computations are based on finite-element models, by the displacement method[1] of the wing and of the fuselage and utilize the force method formulation[2] for considering the wing-fuselage mutual interaction.

As can be seen, the method presented makes use of well-known experimental techniques and analysis methods. The purpose of this paper is to show how these techniques and methods can be utilized for solving such a complex engineering problem as the wing-fuselage structural interaction of the Kfir aircraft. Furthermore, the method presented here shows how to combine the well-established substructuring method for calculations with physical testing.

Combined Method

A schematic flow of the method is shown in Fig. 2. It is composed of five main items, marked in Fig. 2 as 1 to 5, as follows:

1) Performance of static tests on a full-scale wing, supported by a stiff rig, under several load conditions and several different boundary conditions. The displacements at each connection point to the rig were measured and their effects on the wing behavior were experimentally determined simply by superposition.

During the tests, the magnitude of the applied loads was such that a reasonable accuracy of the measurements could be achieved, within the restriction that the maximum stresses remain in the linear range of the material.

2) Construction of a refined finite-element model for the wing structure in order to calculate both displacement patterns and stress distributions. The finite-element model was corroborated by test data of displacements, reactions, and stresses evaluated from the tests on the wing supported in various statically indetermined manners. The influence of the wing flexibilities on the wing-fuselage interaction were later obtained from the finite-element model with statically determined boundary conditions. The test load conditions were not applied on the wing connected to the rig in a statically determined manner because of safety considerations for the structure; i.e., such loads could be much too severe for only a pair of supports out of the four.

In addition, the finite-element model provided a suitable tool for checking the experimental measurements. This was necessary in order to guarantee the reliability of the testing procedure.

3) Performance of static tests on a full-scale fuselage, restrained in a statically determined manner, under different load conditions.

4) Construction of finite-element models of the fuselage frames, to which the wing was attached, and an additional uniaxial lumped model along the center-of-gravity line of the fuselage. The models of the fuselage were less precise than the wing model, since it was realized that the overall influence of the fuselage on the aircraft structural behavior was smaller than the influence of the wing structure.

5) Calculation of the wing-fuselage interaction response. As mentioned, the influence of the wing was obtained from the finite-element model with statically determined boundary conditions. This influence was corroborated previously by testing the wing supported in several statically indetermined boundary conditions. The influence of the fuselage regarding the two test-load conditions was evaluated directly from the experimental measurements. However, for additional load conditions, the influence of the fuselage was obtained from the finite-element models that were previously corroborated for the two test-load conditions.

The question may be raised as to why the present approach was preferred to that of a direct test of a full-scale aircraft, i.e., a fuselage with two wings. The reasons are as follows: 1) Performance of a test on a fuselage with two wings is much more expensive because of the complicated mounting system and the applied load system. 2) The expected accuracy of the measured wing-fuselage reactions in such a full-scale test are presumed to be of the same order as the influence of the fuselage itself. Therefore, there is no advantage in carrying out such a complicated test, as opposed to a simpler test of a wing connected to a stiff rig. 3) The development of a finite-element model suitable for all load conditions can be more assuredly achieved by separate models of the wing with known boundary conditions and the fuselage.

An alternative possibility to obtain measured data which could be extrapolated to other load conditions is by applying unit loads. However, such an approach is not adequate because too high a magnitude of unit loads, which the structure cannot withstand locally, would have to be applied to obtain reasonable accuracy of the measurements. This is also the reason why the testing load conditions were not applied on the wing structure connected to the rig in a statically determined manner.

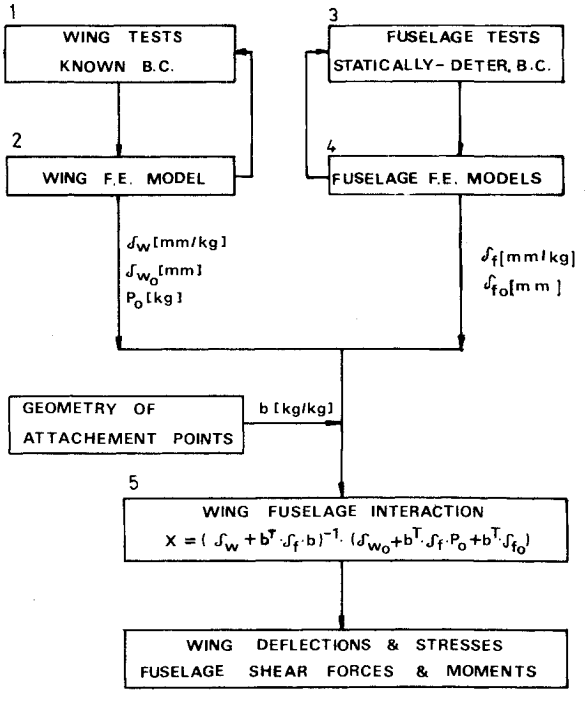

Fig. 2 Schematic flow of the method.

Wing Test Procedure

The wing structure was cantilevered horizontally from a stiff rig by means of the wing-fuselage pickup fittings. Loads were applied by means of six hydraulic jacks and distributed over the structure via whiffle tree elements to bonded rubber pads, as shown in Fig. 3. Forces in the jacks were produced by hydraulic closed-loop servo system, with the controlling feedback signal supplied by the electrical load cells in series with the jacks.

Vertical displacements were measured along several lines in the spanwise and chordwise directions by means of 40 potentiometric-type displacement transducers. Strains were measured by 200 bonded foil strain gages installed on the skins and the spars. Thirty additional strain gages were used for determination of the wing reactions, as explained in the next section.

Several tests were performed on the full-scale wing structure, subjected to different load distributions with different boundary conditions of the wing attachments to the

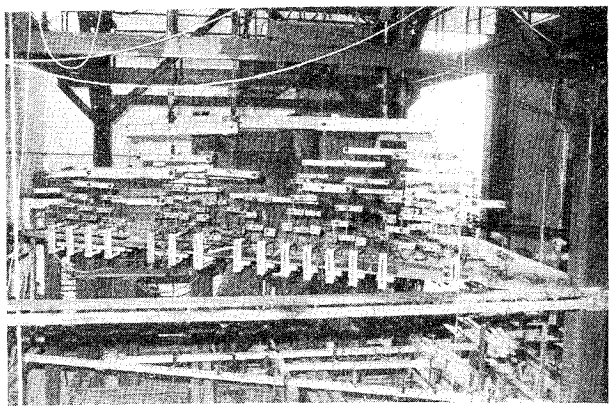

Fig. 3 Wing test system.

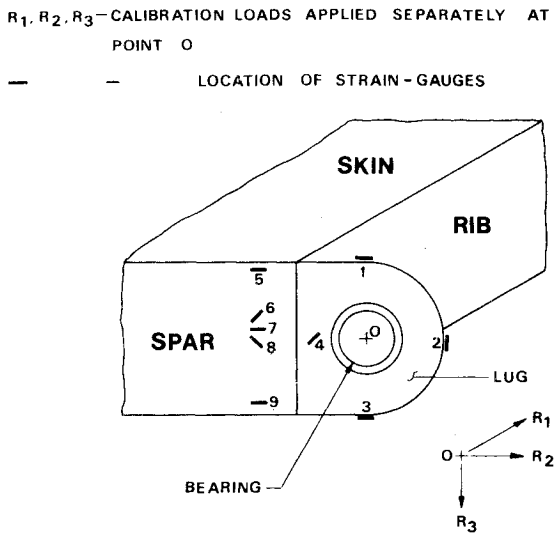

Fig. 4 Locations of calibration loads and strain gages.

rig. Each test was conducted by applying load in discrete increments. Strains and displacements were recorded at each of eleven steps including the zero-load condition at the end of the test.

Measurement of Wing Reactions

Strain gage installations, calibrated on the wing structure, were used for determining the wing pickup reactions. The main difficulties experienced were in selecting suitable representative points for strain gage installation on the pickup lugs. Ideally the required points needed to have high sensitivity, linear behavior, and good repeatability.

To investigate the lug surfaces for suitable locations, as outlined above, the technique of photoelastic coating was used. Figure 4 shows a typical wing fitting connected to frame B or D indicated in Fig. 1. Strain gages 1, 2, 3, and 4 are located at high-strain locations due to at least one of the expected reactions, R_1, R_2, or R_3, shown in Fig. 4. The behavior of these gages was found to deviate slightly from linearity, but their response was repeatable. Gages 1 and 2, for example, were sensitive to load in only one direction. However, this group of gages did not provide sufficient data to solve a set of equations for the fitting loads including a check of accuracy. Therefore, it was necessary to add an additional group of gages, like those indicated at points 5-9 in Fig. 4. These gages showed linear and repeatable behavior. However, they also responded to loads that showed no reaction by the pickup fittings. The contributions of these loads were isolated from the overall reading by means of loading the wing with the full load condition while the fitting in question was disconnected.

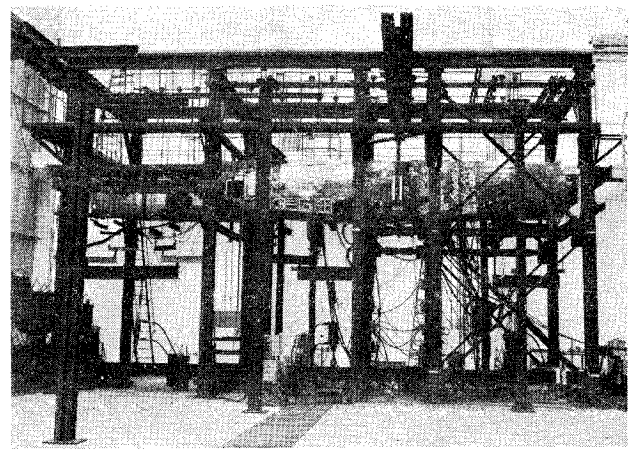

Fig. 5 Fuselage test system.

The wing reactions R_1, R_2, and R_3 were then determined by solving the following set of equations:

$$H \cdot R = \epsilon - \epsilon_0$$

$$(3\times3)\quad(3\times1)\qquad(3\times1)\quad(3\times1) \qquad (1)$$

where matrix H represents strains for unit load for a set of any three out of the five gages (5-9 in Fig. 4). Vector ϵ represents the measured overall strains for the load condition with all fittings connected. Vector ϵ_0 represents the measured strains for the same load condition with the tested fitting being disconnected.

Since nine strain gages were calibrated, it was possible to solve 84 different sets of three equations to determine the three unknown reactions. All the combinations were examined, and those that showed numerically "ill-conditioning" of matrix H were rejected.

The normal standard deviation was calculated using the "well-behaved" sets of combinations. It was found to be less than $\pm 12\%$, which is within the acceptable engineering accuracy.

This reaction determination technique was preferred over the more straightforward technique that considers data from all the nine strain gages simultaneously because the linear behavior of the gages under each load direction was different from the linear behavior under the reversed load direction. Thus, engineering judgment was desired to choose the correct coefficients of matrix H for each set of combinations.

The same method and procedure was used for calibration of the fitting to frame C in Fig. 1. Frame A fitting was much simpler for calibration because is essentially a tie member that was converted to a classical load link.

To cross check the results, an alternative method involving the use of standard-type load cells, connected directly between the wing and rig, was used. Measurements using this method correlate well with results obtained from the strain gage method.

Fuselage Test Procedure

A general view of the fuselage structure with the mounting system is shown in Fig. 5. The fuselage was supported in a statically determined manner at frame A and frame C, as shown in Fig. 1. The support at frame A consisted of two pin-ended columns attached to the wing-fuselage pickup fittings, as shown in Fig. 6a. The support at frame C, shown in Fig. 6b, was more complicated. The support C_1 was constructed to move in the Y direction only, and the support C_2 was completely fixed. The two supports were located just below the wing connection points to apply the high bending moments, due to the wing lift, through the original pins. The wing moments were applied by means of two cantilevered beams as shown in Fig. 6b.

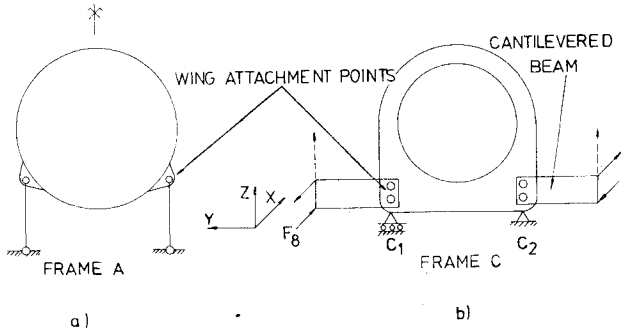

Fig. 6 Fuselage test supports.

The distributed net loads of the two load conditions were applied symmetrically by hydraulic jacks and monitored by electrical load cells. Additional concentrated forces were applied by hydraulic jacks at the free wing-fuselage fittings to determine the fuselage influence coefficients. Measurements of displacements were taken at these fittings by 20 potentiometric displacement transducers. Since the support at frame C was designed to be asymmetric, the average value of the two sides of the fuselage had to be considered.

Ten additional deflection measurements were taken along the bottom centerline of the fuselage to check the mathematical model of the fuselage structure. Five different load distributions were applied and deflection data were obtained for use in the above program. The recording and data reduction were performed automatically using a B&F 256 recording system with a teletype terminal to a time-sharing digital computer.

Modeling of the Wing Structure

The wing structure was idealized as an assembly of finite elements. The NASTRAN computer program[1] was used to perform the calculations. A display-drawn picture of the finite-element model is shown in Fig. 7. The finite-element model includes all the structural members of the wing, including the control surfaces and its servomechanism systems. It consists of 560 nodes, 1500 degrees of freedom, and 2000 elements. The nodes are located half on the upper and half on the lower skin levels at the intersection point of each rib with alternate spars. Additional nodes are located on the skin levels to improve the stress gradient representation.

The upper and lower skin stiffnesses are represented by quadrilateral shear elements that are bordered by uniaxial rod elements. The rod elements represent both the axial stiffness of the spar caps and the inplane stiffnesses of the skins. The cross-sectional area of the rods is calculated so that the moment of inertia of the cross section is preserved. As a result of this, the cross-sectional areas in the model are smaller than the real areas. Therefore, the stresses caused by axial loads are incorrect to some degree. However, the bending stresses are dominant and the overall stresses are only slightly affected. The shear stiffness of panels with variable thicknesses was

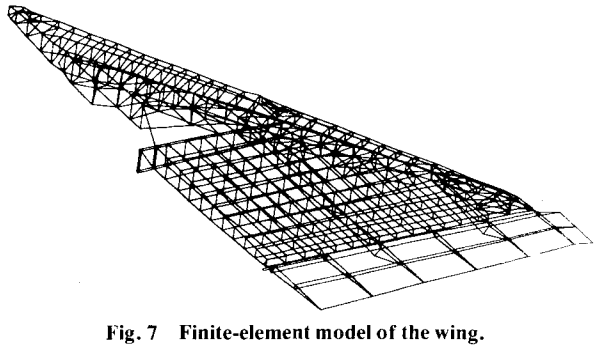

Fig. 7 Finite-element model of the wing.

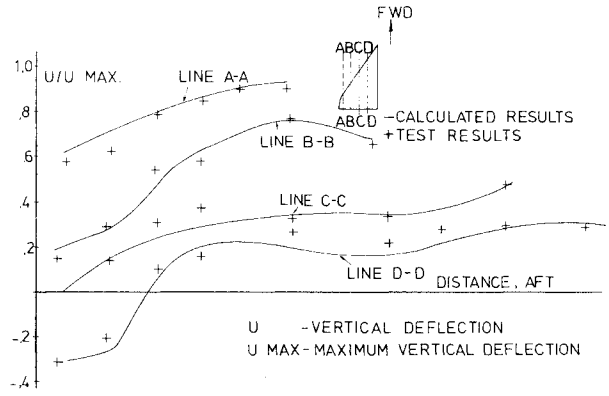

Fig. 8 Comparison of wing deflections.

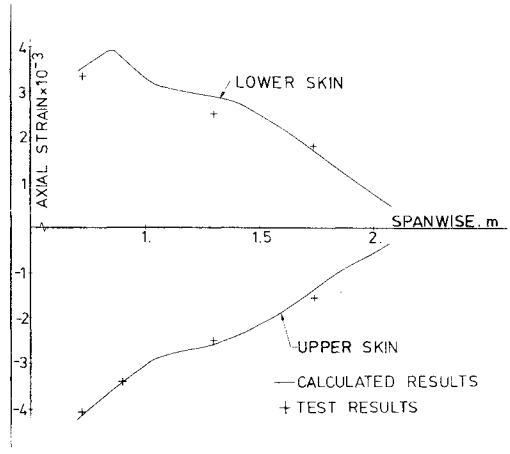

Fig. 9 Comparison of wing main spar strains.

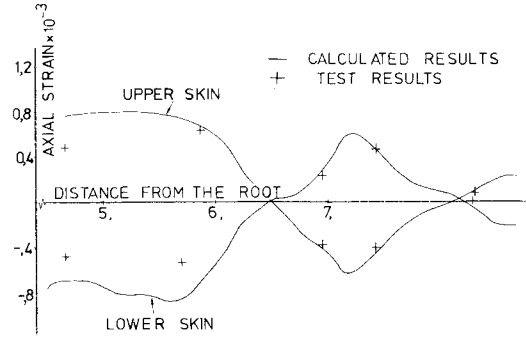

Fig. 10 Comparison of wing front spar strains.

modeled using an average value. The shear stiffness of access panels and vertical webs with lightening holes are modeled using reduced rigidity moduli.

The wing-fuselage fittings, the wing-control surface fittings, and the servomechanism systems are idealized either as space trusses using rod elements or as bending frames. Constant strain triangular elements are used to represent several parts of the wing structure. They are preferred over the combination of shear with rod elements, because of the special local rib and spar orientations. This would require a highly distorted quadrilateral shear element, which would result in appreciable loss of accuracy. However, sufficiently small triangular elements are used to ensure compatibility at the intersection line with each shear element.

Comparison of the wing deflections is shown in Fig. 8 for four chordwise lines. Correlation between test and calculated results is good. Figures 9 and 10 demonstrate the comparison of strain distributions along the main spar and front shear of the wing structure. It can be seen that the calculated values

follow the test data. The calculated reactions of the wing connected to the rig are within the ±10% accuracy of the test results.

Modeling of the Fuselage Structure

The influence of the fuselage structure on the overall structural behavior is smaller than the influence of the wing structure. Thus, instead of constructing a refined model, as was done for the wing structure where each structural element was idealized using the finite-element method, the fuselage structure was modeled using five separate simple models. These models were constructed of bar elements, specified by their cross-sectional areas and moments of intertia, using the NASTRAN computer program.[1]

Four models represent the inplane stiffnesses of frames A, B, C, and D (Fig. 1) to which the wing is attached as shown in Fig. 11a-c. The frames were subjected to three load cases, shown in Fig. 11a-c, which specify the wing-fuselage interaction forces and their induced skin shear flows. The shear flow distributions at frames A, B, and C were calculated by assuming that the skin shear stiffness was small. For frame D, the skin shear stiffness was considered by extension of the mathematical model over three frames in each direction.

Grid 0 shown in Fig. 11a-c is used as a reference point for the frame displacements. It was connected to the frame by two fictitious elements with small cross-sectional area. Its location, along the Z axis, was specified for each frame so that the Maxwell reciprocal theorem for the three load cases, shown in Fig. 11a-c was fulfilled.

The fifth model, shown in Fig. 11d, represents the overall bending stiffness of the fuselage. The boundary conditions at frames A and C were statically determined. The six concentrated forces applied at F_2, F_3, F_8, F_{10}, F_{11}, and F_{12} shown in Fig. 11d were applied separately. They represent the six wing-fuselage redundancies. The distributed loads in Fig. 11d represent the applied airload and inertia load distributions on the fuselage for the considered load condition.

The fuselage was subjected to two types of loads: concentrated loads representing the wing-fuselage reactions and distributed loads simulating the fuselage flight loads. Calculated results due to the concentrated loads agree reasonably with the test results, i.e., the fuselage frames to which the wing is attached, shown in Fig. 11a-c are satisfactorily modeled. Calculated results due to the distributed loads disagree with the test results. This is because the bending stiffness of the fuselage was not determined accurately enough. Therefore, additional tests, under different loading distributions were performed and the mathematical model shown in Fig. 11d was corrected to concur with these test results.

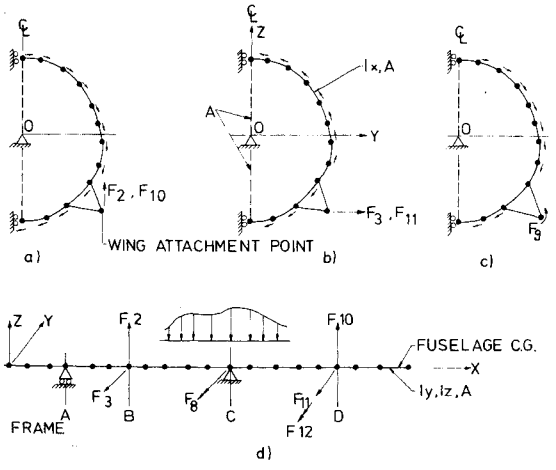

Fig. 11 Finite-element models of the fuselage.

Formulation of the Wing-Fuselage Interaction

Twelve interaction forces act at the wing-fuselage conjunctions, as shown in Fig. 1. Since the statically determined system consists of six forces only, the remaining six forces are redundant variables. Numerical examinations were performed to obtain a well-conditioned matrix for calculation of the statically determined forces. As a result, the redundant force vector X was chosen to be

$$X=\{F_2,F_3,F_8,F_{10},F_{11},F_{12}\} \tag{2}$$

Based on equilibrium considerations the full interaction force vector F can be expressed as follows:

$$\underset{(12\times1)}{F} = \underset{(12\times6)}{b} \cdot \underset{(6\times1)}{X} + \underset{(12\times1)}{P_0} \tag{3}$$

where the rectangular matrix b is the equilibrium transformation matrix, in which each column represents the forces in the statically determined system resulting from a unit redundant force. Since the wing-fuselage attachment points do not lie along a straight line, a coupling also exists between the shear forces and the moments. The vector P_0 is composed of the forces in the statically determined wing supports due to the considered load condition and zeros for the redundant forces.

The continuity condition in the wing-fuselage connection points is

$$\underset{(12\times1)}{r_w} + \underset{(12\times1)}{r_f} = 0 \tag{4}$$

where the vectors r_w and r_f represent the displacements of the attachment points of the wing and the fuselage, respectively. Note that r_w also contains the displacements due to rigid-body motions of the wing.

The wing displacements of the redundant force vector U_w relative to the fixed, statically determined, wing system is given by

$$\underset{(6\times1)}{U_w} = \underset{(6\times6)}{\delta_w} \cdot \underset{(6\times1)}{X} + \underset{(6\times1)}{\delta_{w_0}} \tag{5}$$

where δ_w is the flexibility matrix of the attachment points arising from the redundant forces and δ_{w_0} represents the displacements of the same points caused by the external load condition acting on the wing. Clearly, δ_w and δ_{w_0} are related to the fixed, statically determined wing system. In the present analysis, δ_w and δ_{w_0} are determined by using the wing finite-element model, which was previously corroborated by tests data.

By equating the change of the complementary energy in the fixed and free wing system, caused by virtual redundant forces, one obtains

$$\underset{(6\times1)}{U_w} = \underset{(6\times12)}{b^T} \cdot \underset{(12\times1)}{r_w} \tag{6}$$

The fuselage is supported in a statically determined manner that prevents rigid-body motions. Therefore, the fuselage displacement vector U_f is

$$\underset{(12\times1)}{U_f}=\underset{(12\times1)}{r_f}= \underset{(12\times12)}{\delta_f} \cdot \underset{(12\times1)}{F} + \underset{(12\times1)}{\delta_{f_0}} \tag{7}$$

where δ_f represents the fuselage flexibility matrix at all attachment points. δ_{f_0} represents the displacements of the same fuselage points caused by the external load condition, acting along the fuselage.

By substitution of Eq. (3) into Eq. (7), one obtains

$$U_f = r_f = \delta_f \cdot (b \cdot X + P_0) + \delta_{f_0}$$

By multiplication of the compatibility equation (4) by b^T and substitutions from Eqs. (5), (6), and (8), one obtains an equation for the redundant variables. The solution of the derived equation yields

$$\underset{(6\times 1)}{X} = \underset{(6\times 6)}{-D^{-1}} \cdot \underset{(6\times 1)}{d} \tag{9}$$

where

$$D = \delta_w + b^T \cdot \delta_f \cdot b \tag{10}$$

and

$$d = \delta_{w_0} + b^T \cdot \delta_f \cdot P_0 + b^T \cdot \delta_{f_0} \tag{11}$$

To calculate the additional displacements of the wing due to the flexibility of the fuselage represented by vector V, let us apply again the principle of complementary virtual work. Then one obtains

$$\underset{(n\times 1)}{V} = \underset{(n\times 12)}{\bar{b}^T} \cdot \underset{(12\times 1)}{U_f} \tag{12}$$

where each column of the rectangular matrix $\bar{b}$ represents the wing reactions, in the statically determined supporting system, due to a unit load applied at the nth chosen wing point.

By substitution of Eq. (7) into Eq. (12), one obtains

$$\underset{(n\times 1)}{V} = \underset{(n\times 12)}{\bar{b}^T} \cdot (\underset{(12\times 12)}{\delta_f} \cdot \underset{(12\times 1)}{F} + \underset{(12\times 1)}{\delta_{f_0}}) \tag{13}$$

The following is a summary of the main steps in the solution procedure (see Fig. 2):

1) Compute the wing flexibility matrix δ_w, based on the wing finite-element model with fixed, statically determined, boundary conditions.

2) Obtain the fuselage flexibility matrix δ_f from the fuselage test data.

3) Calculate the equilibrium matrices b and $\bar{b}$ based on the geometric locations of the wing-fuselage attachment points and the statically-determined system.

These steps are common for each load condition. For any given load condition the following additional steps are needed:

Compute the displacement vector δ_{w_0} and the force vector P_0, based on the wing finite-element model with fixed, statically determined, boundary conditions.

5) Compute the displacement vector δ_{f_0}, based on the fuselage model with the statically determined boundary conditions. For the present two load conditions, δ_{f_0} was evaluated directly from the fuselage test data.

6) Calculate the redundant variables X by Eq. (9).

7) Calculate the wing-fuselage interaction force F by Eq. (3).

8) Calculate the fuselage shear force and moment distributions.

9) Calculate wing stresses by superposition of the effect of the real wing-fuselage interaction forces.

10) Calculate displacements at the desired wing points due to the fuselage flexibility by Eq. (13).

Conclusions

A method has been presented for the determination of the wing-fuselage interaction and its effect on the wing displacement and stresses and on the fuselage shear force and moment distributions. This approach combines both numerical calculations and separate full-scale and non-destructive static tests of the wing and of the fuselage. Application of this method to the Kfir aircraft has been described, and it has been found that the wing-fuselage mutual interaction cannot be overlooked. The method can well be applied to other aircraft.

This method was found to be preferable over a direct test of a full-scale aircraft, i.e. a fuselage with two wings, because of the following: 1) this approach is much less complicated and less expensive; 2) good accuracy of the experimentally determined results can be achieved; 3) justification of the finite element models, for the purpose of extrapolating to other load conditions, can be obtained when justification of one complicated model of the whole aircraft is in doubt; 4) reliability of the separate test procedures can be assured utilizing results obtained from the finite element models.

Acknowledgment

The writers gratefully acknowledge the many valuable contributions provided by C. Goldstein, who also reviewed the manuscript.

References

[1] McCormick, W. (ed.), "The NASTRAN User's Manual," NASA SP-222(01), June 1972.

[2] Przemieniecki, J. S., *Theory of Matrix Structural Analysis*, McGraw-Hill, New York, 1963.